Figure 1. (A) Diffusion-weighted magnetic resonance imaging shows acute infarction in the right basal ganglia and insula. (B) Magnetic resonance angiography discloses the occlusion of the right internal carotid artery and middle cerebral artery (arrows). (C) Perfusion lung scintigraphy reveals multiple perfusion defects in both lungs.
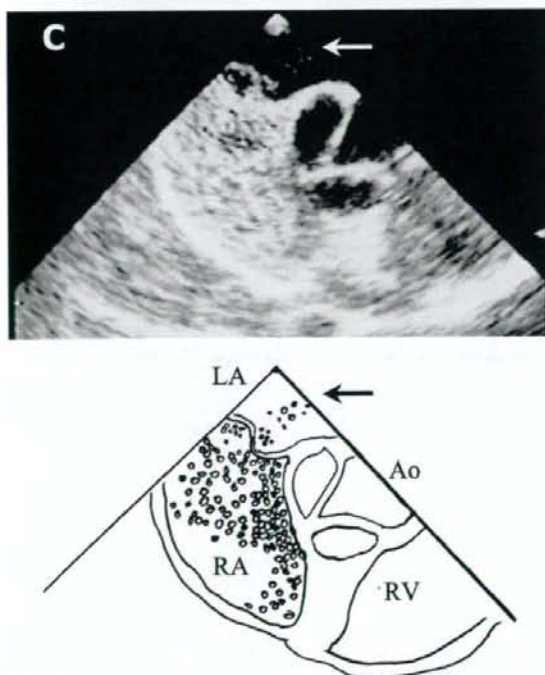

Figure 2. Contrast transesophageal echocardiographic examination. Microbubbles fill the right atrium and appear in the left atrium through a patent foramen ovale without Valsalva maneuver (arrow). LA, left atrium; RA, right atrium; RV, right ventricle; Ao, aorta.

Discussion

PCE is a unique ischemic stroke in which emboli originating from the venous system reach the cerebral arterial circulation via the R-L shunt, such as PFO (1). Recently, Yasaka et al advocated the diagnostic criteria for PCE (2). According to their criteria, the diagnosis of PCE is definitive, if the following five conditions are satisfied: 1) neuroradiological demonstration of brain infarction, 2) the presence of PFO, 3) the presence of venous thrombosis, 4) temporal profile or neuroradiological findings indicating embolic mechanism, and 5) the absence of other embolic sources. In the present case, all these conditions are satisfied, and hence it can be said that the left ICA occlusion causing relatively large cerebral infarction was produced by PCE mechanisms.

According to autopsy studies (3), the mean diameter of PFO is 4.9 mm. The diameter of PFO is, thus, considerably large as compared with cerebral arterial diameter. The mean internal diameter of ICA and MCA was reported to be 3.6 mm and 2.5 mm, respectively (4). Provided large emboli with 3-4 mm in diameter can pass through PFO easily, then the major cerebral arteries, such as ICA or MCA, may be readily occluded resulting in the formation of large cerebral infarction. Nevertheless, the previous studies suggest that cerebral infarction caused by PCE mechanisms is generally small in size (5, 6). To our best knowledge, only five cases with PFO were reported to have large cerebral infarction previously (7-11). The present communication is the first to

report a definitive PCE case in which ICA occlusion was clearly demonstrated by MR angiogram.

It should be emphasized that four of the above-mentioned five PFO cases were associated with pulmonary thromboembolism (7, 8, 10, 11) as found in the present case. Pulmonary thromboembolism increases the pulmonary vascular resistance and inevitably elevates the right atrial pressure. In the present case, the pulmonary arterial pressure was increased to approximately 80 mmHg in the acute phase of stroke due to pulmonary thromboembolism. In this acute phase, the R-L shunting was constantly observed without Valsalva maneuver on TEE or TCCS. On the other hand, in the chronic phase at which the pulmonary arterial pressure decreased to 46 mmHg, the R-L shunting was no longer detected even during Valsalva maneuver. The fact strongly suggests that the passage of embolus through PFO is largely in-fluenced by the right heart pressure. Under normal right heart pressure, the R-L shunting may not be provoked even with Valsalva maneuver. However, under high right heart pressure caused by pathological condition such as pulmonary thromboembolism, the shunt flow may pass through PFO easily allowing the passage of large embolus.

In conclusion, the present case suggests that the major cerebral artery can be occluded by PCE mechanisms if the right heart pressure is increased to enormously high level due to pulmonary thromboembolism. In patients with PCE presenting a large-sized infarction, pulmonary thromboembolism should be aggressively screened. The evaluation of right heart pressure and R-L shunting state in patients with PCE during the acute stage may further clarify clinical characteristics of PCE.

References

1. Amarenco P. Cryptogenic stroke, aortic arch atheroma, patent foramen ovale, and the risk of stroke. Cerebrovasc Dis 20: 68-74, 2005.
2. Yasaka M, Otsubo R, Oe H, Minematsu K. Is stroke a paradoxical embolism in patients with patent foramen ovale? Intern Med 44: 434-438, 2005.
3. Hagen PT, Scholz DG, Edwards WD. Incidence and size of patent foramen ovale during the first 10 decades of life: an autopsy study of 965 normal hearts. Mayo Clin Proc 59: 17-20, 1984.
4. Wollschlaeger G, Wollschlaeger PB, Lucas FV, Lopez VF. Experience and result with postmortem cerebral angiography performed as routine procedure of the autopsy. Am J Roentgenol Radium Ther Nucl Med 101: 68-87, 1967.
5. Becker K, Skalabrin E, Hallam D, Gill E. Ischemic stroke during sexual intercourse: a report of 4 cases in persons with patent foramen ovale. Arch Neurol 61: 1114-1116, 2004.
6. Steiner MM, Di Tullio MR, Rundek T, et al. Patent foramen ovale size and embolic brain imaging findings among patients with ischemic stroke. Stroke 29: 944-948, 1998.
7. Playfor SD, Smyth AR. Paradoxical embolism in a boy with cystic fibrosis and a stroke. Thorax 54: 1139-1140, 1999.
8. Narimatsu E, Kawamata M, Hase M, Kurimoto Y, Asai Y, Namiki A. Severe paradoxical intracranial embolism and pulmonary emboli during hip hemiarthroplasty. Br J Anaesth 91: 911-913, 2003.
9. Willinek WA, Strunk H, Born M, Remig J, Becher H, Schild H. Popliteal venous aneurysm with paradoxical embolization in a patient with patent foramen ovale. Circulation 104: E60-61, 2001.
10. Kinney TB, Rose SC, Lim GW, Auger WR. Fatal paradoxic embolism occurring during IVC filter insertion in a patient with chronic pulmonary thromboembolic disease. J Vasc Interv Radiol 12: 770-772, 2001.
11. Claver E, Larrousse E, Bernal E, Lopez-Ayerbe J, Valle V. Giant thrombus trapped in foramen ovale with pulmonary embolus and stroke. J Am Soc Echocardiogr 17: 916-918, 2004.

Isolated Hemifacial Sensory Impairment with Onion Skin Distribution Caused by Small Pontine Hemorrhage

N. Toratani   H. Moriwaki   B. Hyon   H. Naritomi

Department of Cerebrovascular Medicine, National Cardiovascular Center, Osaka, Japan

Dear Sir,

Isolated trigeminal sensory neuropathy due to pontine hemorrhage has only been found in a few previous cases [1–4]. In these, the hemorrhage affected either the principal sensory nucleus [1, 2] or the trigeminal nerve roots [3, 4] and produced facial sensory impairments along the ophthalmic (V1), maxillary (V2) and/or mandibular (V3) nerve dermatome. We report a patient with a small pontine hemorrhage that affected the upper part of the spinal trigeminal nuclei, mainly the nucleus oralis and interpolaris. She developed isolated facial tactile sensory impairment with 'onion skin' distribution in the absence of other neurological deficits. Onion skin type facial sensory impairment caused by these upper spinal trigeminal nuclei due to stroke has never been previously reported.

Case Report

A 61-year-old woman suddenly felt numbness around the right side of her lips while talking on the telephone. She experienced neither headache nor vomiting. She had a history of hypertension and hyperlipidemia but received no medical treatment. She was admitted to our hospital 1 h after onset. At the time of admission, her blood pressure was 200/114 mm Hg, while the heart beats were 108 per

minute and regular. Neurological examinations revealed an alert and well-oriented woman with isolated tactile sensory impairment over the right trigeminal distribution including the oral cavity. Pain and temperature sensations were not impaired. The hypesthesia showed so-called onion skin distribution and was least intense in the perioral and perinasal areas and most prominent in the most peripheral parts of the face, such as the forehead and chin. Corneal sensation and corneal reflex were well preserved. No weakness of the masseteric muscle or jaw deviation was observed. Taste sensation was normal. There was no abnormality in cranial nerves, coordination or body sensation, except for the face.

Brain CT performed on admission and 1.5 h after onset demonstrated a small, high-density area at the right pontine tegmentum (fig. 1). The diameter of the hematoma was less than 1 cm and did not enlarge on a second CT performed 6 h after onset. T_1-weighted MRI on the seventh day showed a column-shaped hematoma in areas extending from the middle part to the lower portion of the pons and accompanied by a smaller sublesion (fig. 2A–C). The hematoma did not reach the medulla oblongata, as confirmed by coronal MRI. MR angiography on the seventh day disclosed no abnormality suggestive of arteriovenous malformation, aneurysm or

cavernous angioma. The diagnosis of hypertensive pontine hemorrhage was established on the basis of such imaging studies. She was discharged on day 11, at which time her facial hypesthesia was mild in degree. Three months thereafter, her facial hypesthesia was confined to the areas around the right side of the lips.

Discussion

Pontine hemorrhage presenting a trigeminal neuropathy is usually associated with other cranial nerve deficiencies. Even in cases of small hematoma localized in the tegmentum, neurological examination usually reveals a variety of symptoms depending on the magnitude of basilar involvement, such as oculomotor abnormalities, ataxia, action tremor, ipsilateral miosis, hemiparesis or facial numbness [5]. Isolated trigeminal sensory neuropathy is seldom observed in cases of pontine hemorrhage. To the best of our knowledge, only 4 such cases have been reported previously [1–4] (table 1). In these 4 cases, the lesions affected the principal sensory nucleus or the trigeminal nerve roots, and all of the facial sensory impairments were observed along the V1, V2 or V3 dermatomes.

The trigeminal nerve contains both sensory and motor components. The ma-

Naomi Toratani
Department of Cerebrovascular Medicine
National Cardiovascular Center
5-7-1 Fujishirodai, Suita, Osaka 565-8565 (Japan)
Tel. +81 6 6833 5012, Fax +81 6 6872 7486, E-Mail tora@hsp.ncvc.go.jp

Fig. 1. Brain CT, obtained 1.5 h after onset of symptoms, discloses a small, high-density area (arrow) in the medial portion of the right pontine tegmentum.
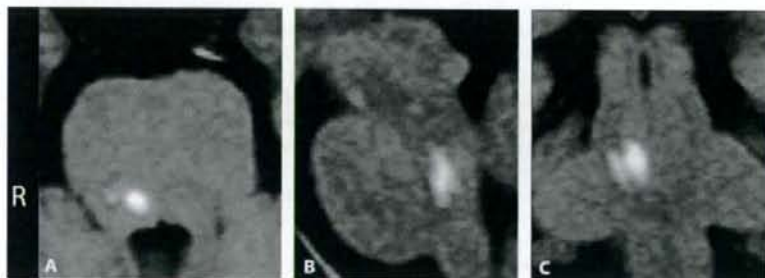
Fig. 2. T$_1$-weighted MR images obtained on the seventh day. **A** Transaxial image discloses hematoma at the pontine tegmentum, the diameter of which is smaller than 1 cm. **B, C** The sagittal and coronal images demonstrate that the hematoma is column-shaped, extending from the middle pons to the lower pons and accompanied by a smaller sublesion.

Table 1. Reported cases of pontine hemorrhage with isolated trigeminal sensory neuropathy

Authors and year	Age years	Sex	Distribution	Location of the lesion
Holtzman et al. [1], 1987	45	M	V2, V3	trigeminal principal sensory nucleus
Kim et al. [2], 1994	31	M	V1 < V2, V3	trigeminal nerve root and trigeminal principal sensory nucleus
Komiyama et al. [3], 1993	49	M	V1	trigeminal nerve root
Almeida et al. [4], 1999	62	M	V1	trigeminal nerve root
The present case	61	F	V1~V3 'onion skin' pattern	nucleus oralis or interpolaris of trigeminal spinal nucleus

jority of trigeminal sensory fibers conveying tactile sensation does not descend but enters the principal sensory nucleus. Other trigeminal sensory fibers carrying pain and temperature sensations descend in the trigeminal tract and enter the spinal trigeminal nucleus. The spinal trigeminal nucleus consists of 3 components – the nucleus oralis, nucleus interpolaris and nucleus caudalis – which are located along the longitudinal axis of the brain stem [6–8]. Among these nuclei, the fibers carrying pain and temperature sensations enter the nucleus caudalis, which is located at the most caudal part of the spinal trigeminal nucleus. The somatotopic representation of the face within the nucleus caudalis is in a segmental distribution similar to onion skin: the perioral areas of the face are represented by the rostral portion of the nucleus, and more outer areas of the face are represented by the caudal portion of the nucleus. Therefore, lesions affecting the nucleus caudalis at the medulla oblongata may cause onion skin type sensory impairment, as occasionally observed in cases of syringobulbia. On the other hand, the functions of the other 2 nuclei – the nucleus oralis and interpolaris – still remain unclear. Fibers carrying tactile sensation mainly enter the principal sensory nucleus and partly so the upper part of the spinal

trigeminal nucleus – the nucleus oralis and interpolaris [9]. The tactile representation of the face within the nucleus oralis and interpolaris remains unclear.

In the present case, isolated tactile sensory impairment with onion skin distribution was observed in the hemifacial area ipisilateral to the side of the small pontine hemorrhage. According to the CT and MRI studies, the hematoma was located more medially to the principal sensory nucleus and affected the upper part of the spinal trigeminal nucleus, such as the nucleus oralis and interporalis. The onion skin type hypesthesia is unlikely to be caused by lesions of the principal sensory nucleus. The present case suggests that the onion skin type hypesthesia may be caused by lesions in the nucleus oralis or interpolaris. The somatotopic representation of the face in the nucleus oralis and interpolaris may be in a segmental, onion-skin-like distribution pattern similar to that in the nucleus caudalis.

References

1 Holtzman RN, Zablozki V, Yang WC, Leeds NE: Lateral pontine tegmental hemorrhage presenting as isolated trigeminal sensory neuropathy. Neurology 1987;37:704–706.

2 Kim JS, Lee MC, Kim HG, Suh DC: Isolated trigeminal sensory change due to pontine hemorrhage. Clin Neurol Neurosurg 1994; 96:168–169.

3 Komiyama M, Fu Y, Yagura H, Yasui T, Khosla VK, Berlit P: Pontine hemorrhages presenting as trigeminal neuropathy: report of three cases – Trigeminal neuropathy in pontine hemorrhage. Neurol Med Chir 1993;33: 234–237.

4 Almeida S, Chalk C, Minuk J, Del Carpio R, Guerin M, Levental M: Isolated trigeminal neuropathy due to trigeminal nerve root hemorrhage. Can J Neurol Sci 1999;26:204–206.

5 Chung CS, Park CH: Primary pontine hemorrhage: a new CT classification. Neurology 1992;42:830–834.

6 Carpenter MB: Core Text of Neuroanatomy, ed 4. Baltimore, Williams & Wilkins, 1991, pp 176–182.

7 Wall PD, Taub A: Four aspects of trigeminal nucleus and a paradox. J Neurophysiol 1962; 25:110–126.

8 Chiang CY, Hu B, Hu JW, Dostrovsky JO, Sessle BJ: Central sensitization of nociceptive neurons in trigeminal subnucleus oralis depends on integrity of subnucleus caudalis. J Neurophysiol 2002;88:256–264.

9 Goto F, Aamano T: Functional Neuroanatomy for Clinical Practice, ed 1. Tokyo, Chugai Igaku, 1992, pp 20–21.

Microembolic Signals within 24 Hours of Stroke Onset and Diffusion-Weighted MRI Abnormalities

Makoto Nakajima[a]   Kazumi Kimura[b]   Atsuko Shimode[a]   Fumio Miyashita[a]
Makoto Uchino[c]   Hiroaki Naritomi[a]   Kazuo Minematsu[a]

[a]Cerebrovascular Division, Department of Medicine, National Cardiovascular Center, Osaka, [b]Stroke Center,
Kawasaki Medical School, Kurashiki, and [c]Department of Neurology, Kumamoto University School of Medicine,
Kumamoto, Japan

Abstract

Background: The clinical relevance of the microembolic signals (MES) detected by transcranial Doppler sonography (TCD) in acute stroke remains unclear. In a prospective study the authors analyzed the relationship between MES and the findings on diffusion-weighted magnetic resonance imaging (DWI) in acute stroke patients. **Methods:** We performed TCD for a period of 30 min to detect MES in patients within 24 h of stroke onset, and DWI was done within the initial 7 days. MES were assessed from Doppler waves obtained from the middle cerebral artery contralateral to the side of the neurological deficits. The acute ischemic lesions observed on DWI were classified by their diameter (small, medium or large) and by their site (cortical, superficial perforator territory, internal borderzone or deep perforator territory). **Results:** We obtained Doppler waves from 39 vessels in 37 patients; 2 patients had bilateral deficits. MES were detected in 12 vessels (MES-positive group) and not detected in 27 vessels (MES-negative group). No significant differences in clinical features were observed between the 2 groups. The number of small lesions was significantly higher in the MES-positive group than in the MES-negative group (p = 0.02). The numbers of cortical and superficial perforator infarcts were significantly higher in the MES-positive group than in the MES-negative group (p = 0.002 and 0.02, respectively). **Conclusion:** In acute ischemic stroke, MES detected by TCD in the acute phase may produce small cortical and subcortical lesions found on DWI.

Copyright © 2007 S. Karger AG, Basel

Introduction

Microembolic signals (MES) have been detected by transcranial Doppler (TCD) in patients with carotid diseases, atrial fibrillation, prosthetic cardiac valves and carotid angiography, as well as intraoperatively in patients undergoing cardiac or carotid surgery [1–10]. MES is detected in 4–56% of acute stroke patients [11–17]. However, the clinical relevance of MES in acute stroke remains unclear. Although they are usually asymptomatic, small emboli may cause small ischemic brain lesions [18, 19].

Makoto Nakajima
Department of Medicine, Kumamoto Rosai Hospital
1670, Takehara-machi, Yatsushiro
Kumamoto 866-8533 (Japan)
Tel. +81 965 33 4151, Fax +81 965 32 4405, E-Mail rosainakazima@ybb.ne.jp

Diffusion-weighted magnetic resonance imaging (DWI) detects hyperacute ischemic lesions more sensitively than conventional CT and conventional magnetic resonance (MR) imaging [20, 21]. DWI has a high sensitivity and specificity in the acute setting of stroke [22]. It is also useful for the diagnosis of stroke within 6 h of symptom onset [23]. Although we and other authors have reported that there is a relationship between MES and DWI, in most of the studies, TCD was performed within ≥2 days of stroke onset, and the subjects were only those who had large artery disease or other emboligenic diseases [24, 25]. In these reports MES were obtained from both middle cerebral arteries (MCAs), which included the artery ipsilateral to the side of the deficits.

To evaluate the relationship between MES and the ischemic lesions more precisely, we did a prospective study to detect MES in patients with ischemic stroke or transient ischemic attack (TIA) by doing a TCD within 24 h of onset, and then by analyzing the relationship between the MES from only the MCA contralateral to the side of the deficits and the lesions found on DWI.

Patients and Methods

We conducted a prospective study of 56 consecutive patients with carotid ischemic stroke who were admitted to our hospital within 24 h of stroke or TIA onset between September 2002 and April 2003.

The following clinical data were collected from all patients: (1) patient age and gender; (2) the number of MES detected by TCD from the MCA contralateral to the side of the neurological deficits; (3) National Institutes of Health Stroke Scale (NIHSS) score [26] on admission; (4) the presence of vascular risk factors, including hypertension, diabetes mellitus, hypercholesterolemia and current cigarette smoking; (5) history of stroke; (6) emboligenic cardiac and aortic diseases; (7) significant arterial diseases corresponding to the neurological deficits; (8) laboratory parameters on admission (white blood cell count, hematocrit, platelet count, fibrinogen, C-reactive protein); (9) blood coagulation factors (thrombin-antithrombin III complex), D-dimer, antithrombin III on admission; (10) the interval of time between stroke onset and the TCD study or MR imaging; (11) the administration of anticoagulant agents, including heparin and warfarin, and antiplatelet agents, including aspirin and ticlopidine, at the time of the TCD study.

The TCD study was performed using a DWL Multidop X with a 2.5-MHz probe within 24 h of stroke or TIA onset. With the patients supine, bilateral MCA recordings for 30 min at a depth of 45–55 mm were done. The MES were based on the Doppler waves obtained from the MCA contralateral to the side of the neurological deficits. The TCD probe was held in place with an elastic headband to reduce the possibility of a movement artifact. MES were defined according to the standard consensus criteria [27] as being 6 dB above the background threshold. Blinded 'offline' validation of suspected MES was done by 2 of the authors (M.N. and A.S.), who reviewed the digital audiotape recordings, instead of relying solely on automatic counting by DWL software.

To detect potential cardiac sources of emboli, all patients were examined using a 12-lead electrocardiograph (ECG), 24-hour ECG monitoring and transthoracic echocardiography. The following potential emboligenic cardiac diseases were considered: nonvalvular atrial fibrillation, acute myocardial infarction, previous myocardial infarction with intraventricular thrombus, mitral valve diseases, prosthetic cardiac valve, dilated cardiomyopathy, patent foramen ovale and cardiac tumor. Potential aortogenic sources of emboli or patent foramen ovale were evaluated in 27 patients by transesophageal echocardiography. Localized raised lesions in the aorta with a maximal intima-medial thickness >4.0 mm and an obviously irregular surface, a broad acoustic shadow, or mobile plaque were defined as potential aortic sources of emboli.

All patients underwent color-flow duplex carotid ultrasonography on the day of admission. Conventional cerebral angiography and/or MR angiography was performed in all patients. The stenosis was graded according to the method used by the North American Symptomatic Carotid Endarterectomy Trial [28]. Significant arterial disease was identified if a stenosis >50% or an ulcerated plaque was found in the affected artery that corresponded to the neurological deficits.

MR imaging was performed within 7 days of stroke onset, using a 1.5-tesla system equipped with single-shot echo planar imaging to obtain rapid diffusion images. MR studies included axial T_1-weighted, axial T_2-weighted and DWI sequences. The imaging parameters were 4000/103 (TR/TE), 128 × 128 matrix, 230-mm field of view, and 4 mm slice thickness with a 2-mm gap between the slices. Two b-values were used: 0 and 1,000 s/mm². Diffusion gradients were applied in successive scans in each of the x, y and z directions, and DWI images were formed from the average of these values. The criterion for the diagnosis of acute infarcts on DWI was focal hyperintensity, judged not to be due to normal anisotropic diffusion or magnetic susceptibility artifacts. Each MRI was assessed by 2 authors (M.N. and K.K.); only those lesions that both assessors identified were judged to be new ischemic lesions. We classified the acute ischemic lesions found on DWI by size (small, <10 mm in diameter; medium, 10–30 mm in diameter, or large >30 mm in diameter) and by their locations (cortical, superficial perforator territory, internal borderzone or deep perforating artery territory). Cortical lesions were defined as the lesions including cortical ribbon (fig. 1A). Subcortical lesions were further split into superficial perforator lesions according to the templates of Bogousslavsky and Regli [29] (fig. 1B), and internal borderzone lesions according to the schematic templates by Del Sette et al. [30] and Lee et al. [31] (fig. 1C). The outermost limit of superficial perforator lesions was taken to be the cortical ribbon; the innermost limit was the corona radiata at the level of the deep perforator. Internal borderzone lesions were defined as hyperintense areas in the vascular internal borderzone, where the border between the deep and superficial perforating arteries divides the lesion into 2 approximately equal sections. We excluded lesions located within the borderzone area between the MCA and the anterior cerebral artery or the MCA and the posterior cerebral artery. The deep perforating artery territory was defined as the regions including deep corona radiata, putamen, globus pallidus, internal capsule and caudate head (fig. 1D).
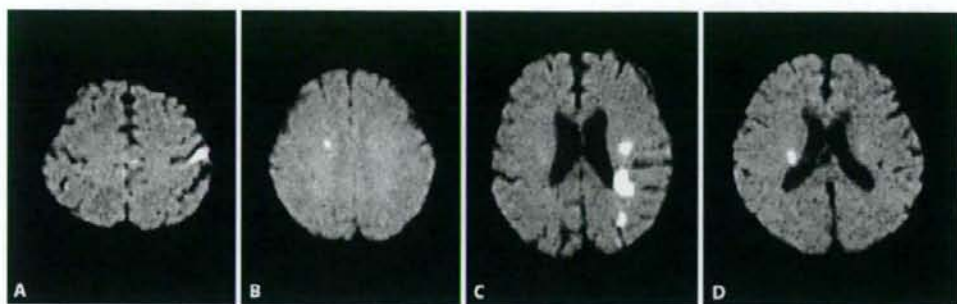
Fig. 1. Examples of location of infarct. **A** Cortical infarcts. **B** Superficial perforator infarcts. **C** Internal boderzone infarcts. **D** Deep perforating artery territory infarcts.

The Mann-Whitney U test was used to detect statistically significant differences in age, NIHSS score, and interval between stroke onset and TCD or MR assessment between the groups. All other findings were assessed by Fisher's exact test. In addition, we analyzed the relationship between the number of MES on TCD and the presence of lesions on DWI by Spearman's correlation test. Statistical analysis was performed using a commercially available software package (Stat-View, version 5, SAS Institute Inc., USA). p values <0.05 were considered statistically significant.

Results

We analyzed 39 MCAs in 37 patients (34 men, 3 women, age 69 ± 10 years); 19 patients were excluded from the initial 56 patients, as they lacked temporal windows on the side of interest (n = 16) or had no available MR images due to prior pacemaker implantation (n = 3). Both MCAs were evaluated in 2 of the 37 patients because they showed bilateral neurological deficits. The mean time interval between stroke onset and TCD assessment was 11.0 ± 6.4 h, (median 8.2, range 2.3–24.0); the mean time interval between stroke onset and MR assessment was 33.9 ± 29.7 h (median 27.9, range 12.3–183.5).

The MES-positive group consisted of 11 patients in whom MES were detected in 12 MCAs (30.8%), while the MES-negative group consisted of 26 patients in whom no MES were detected in 27 vessels (69.2%). No significant differences were observed between the 2 groups with respect to clinical features, including NIHSS score on admission, emboligenic diseases, arterial diseases and use of either oral or transvenous antithrombotic agents. Laboratory parameters and blood coagulation factors on admission did not differ between the 2 groups either (table 1). Transesophageal echocardiography was performed

in 7 of 10 patients in the positive group and 20 of 26 patients in the negative group. Although certain emboligenic diseases (arterial diseases, heart diseases or complicated lesions in the aortic arch) were seen more frequently in patients in the MES-positive group, the differences between the MES-positive and -negative groups were not statistically significant.

The number of small lesions was significantly higher in the MES-positive group (3.5 ± 4.5) than in the MES-negative group (0.7 ± 1.0, p = 0.02), whereas the numbers of medium lesions (0.9 ± 1.5 MES-positive vs. 0.2 ± 0.4 MES-negative, p = 0.07) and large lesions (0.3 ± 0.5 MES-positive vs. 0.4 ± 0.5 MES-negative, p = 0.83) did not differ between the 2 groups (fig. 2). The number of cortical infarcts was significantly higher in the MES-positive group (3.8 ± 4.3) than in the MES-negative group (0.7 ± 0.8, p = 0.002). The number of superficial perforator lesions was significantly higher in the MES group (0.8 ± 0.9 vs. 0.3 ± 0.3, p = 0.02), while the number of internal borderzone lesions did not differ between the 2 groups (0.2 ± 0.4 vs. 0.3 ± 0.7, p > 0.99). No differences were seen in the number of deep perforator territory infarcts (0.2 ± 0.4 MES-positive vs. 0.3 ± 0.5 MES-negative, p = 0.66, fig. 3) between the 2 groups. The number of MES had a weak association with the number of DWI lesions (p = 0.003, ρ = 0.605, fig. 4).

MES was detected in 1 patient with a single deep perforating artery infarct. He is a 72-year-old man with hypertension and diabetes mellitus, who showed pure motor stroke on the right side. The coagulation and fibrinolytic markers showed no abnormality. His symptoms did not progress during his hospital stay.

Nakajima/Kimura/Shimode/Miyashita/
Uchino/Naritomi/Minematsu
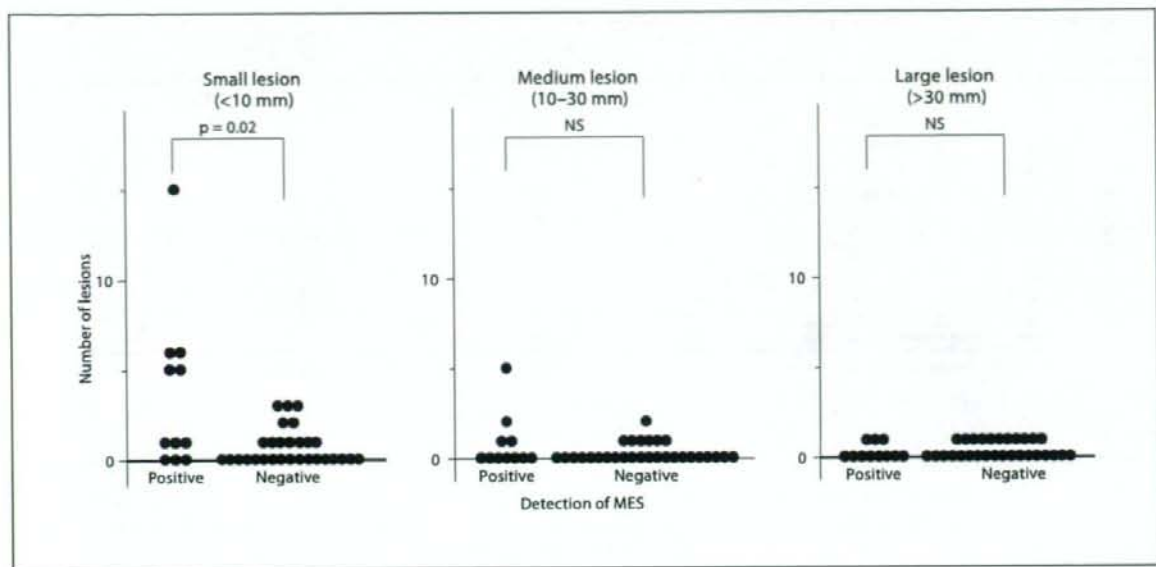
Fig. 2. On DWI, small ischemic lesions were more frequent in the MES-positive group than in the MES-negative group. However, the frequencies of medium lesions and large lesions did not differ between the 2 groups.

Table 1. Patient characteristics in MES-positive group and MES-negative group

	Detection of MES		p
	positive (n = 11)	negative (n = 26)	
Age[a]	68 (50–79)	68 (50–88)	0.48
Male sex	10 (91%)	24 (92%)	>0.99
Hypertension	10 (91%)	16 (62%)	0.12
Diabetes	3 (27%)	10 (38%)	0.71
Hyperlipidemia	3 (27%)	10 (38%)	0.71
Smoking	7 (64%)	18 (69%)	>0.99
Previous stroke	2 (18%)	12 (46%)	0.15
Arterial stenosis (≥ NASCET 50%)	3 (27%)	4 (15%)	0.40
Atrial fibrillation	4 (36%)	6 (23%)	0.44
Potential embolic source	4/7 (57%)	10/20 (50%)	>0.99
Intravenous antithrombotic agent	4 (36%)	12 (46%)	0.72
Oral antithrombotic agent	4 (37%)	13 (50%)	0.50
Time interval from onset to TCD study[a]	11.8 (2.5–24.0)	7.2 (2.3–24.0)	0.19
White blood cell, × 10³/μl[a]	9.1 (3.7–14.6)	7.4 (3.0–13.2)	0.61
Hematocrit, %[a]	41.2 (37.5–47.7)	39.7 (18.9–47.4)	0.34
Platelet, × 10³/μl[a]	182 (103–258)	210 (93–420)	0.27
Fibrinogen, mg/dl[a]	353 (251–455)	332 (179–582)	0.67
C-reactive protein, mg/l[a]	0.36 (0.11–10.40)	0.24 (0.06–5.39)	0.21
Thrombin-antithrombin III complex, μg/l[a]	1.6 (0.5–19.5)	1.7 (0.2–15.1)	0.59
D-dimer, ng/ml[a]	1.0 (0.5–14.5)	0.9 (0.1–11.0)	0.31
Antithrombin III, %[a]	84.7 (75.8–104.6)	86.0 (71.6–136.9)	0.87

[a] Median (range). NASCET = North American Symptomatic Carotid Endarterectomy Trial.
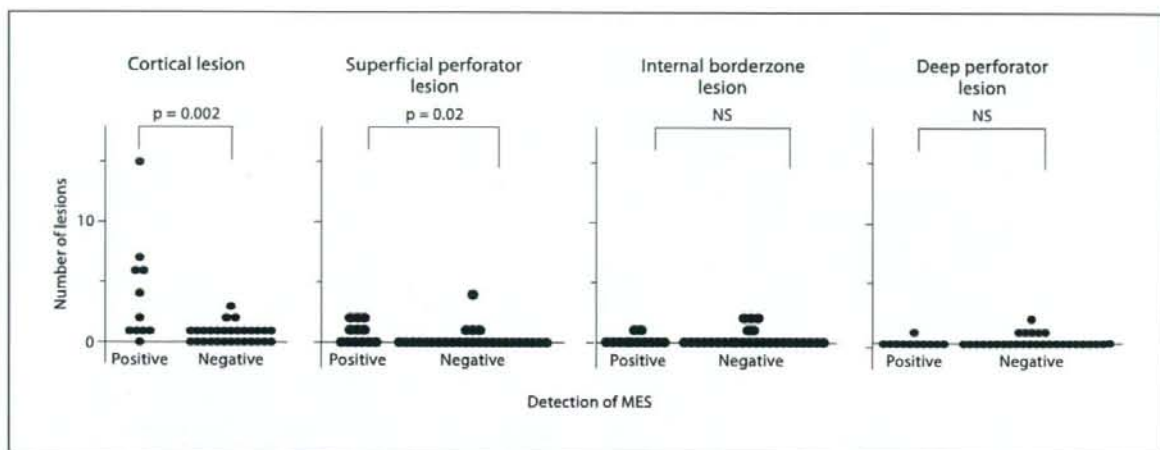
Fig. 3. Cortical lesions and superficial perforator lesions were more frequently seen on DWI in the MES-positive group than in the MES-negative group, while the frequencies of subcortical lesions and lesions in the perforating arterial territory did not differ between the 2 groups.
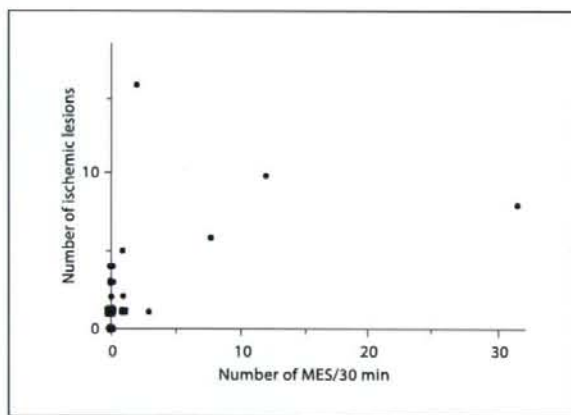
Fig. 4. Relationship between the number of MES and the number of ischemic lesions seen on DWI. A mild association is seen between them (p = 0.003, ρ = 0.605).

Discussion

The presence of MES indicates that a stroke may be embolic in origin. Multiple lesions on DWI would also relate to multiple emboli or the breakup of an embolus. Some authors have discussed the relationship between multiple lesions and stroke etiology [32, 33]. In this study,

we confirmed the relationship between the detection of MES in the MCA contralateral to the side of the deficits and abnormal lesions found on DWI in the ipsilateral cerebrum. Our results are similar to the results of past studies suggesting that MES have a relationship with the small cortical lesions seen on DWI [24, 25], and our results extend this relationship to include patients with acute ischemic stroke within 24 h of stroke onset.

While the relationship between ischemic lesions in the cerebral cortex and an embolic mechanism is broadly recognized, subcortical infarcts may have a combined mechanism, including a hemodynamic mechanism. Our study showed a suggestive result: subcortical lesions in the superficial perforator associated with the detection of MES, while internal borderzone lesions did not. In previous reports, some subcortical infarcts including the centrum ovale are thought to be associated with cardiac or arterial diseases [33, 34]. Others have described that deep subcortical infarcts including the internal borderzone may be caused by a hemodynamic mechanism or a combination of hypoperfusion and microemboli in intracranial arteries with severe stenosis [35, 36]. Our result may emphasize the difference between superficial perforator infarcts and internal borderzone infarcts, although not confirmative because of small sample size.

We found that the association between the number of MES and the number of DWI lesions was weak (ρ = 0.605), while Wong et al. [35] reported a stronger asso-

Nakajima/Kimura/Shimode/Miyashita/
Uchino/Naritomi/Minematsu

ciation. This difference can be explained by differences between the 2 study populations; we assessed consecutive stroke patients with various etiologies, while Wong et al. evaluated only patients with stenotic lesions in the proximal segment of the MCA. Therefore, our result suggested an association not only between MES and embolism, but also between MES and other stroke mechanisms, that is, platelet hyperactivation or hypercoagulability.

One patient showed MES in the MCAs bilaterally, though he had no potential emboligenic diseases. On DWI this patient was found to have a single deep perforating artery infarct, indicating that embolism is the likely cause of a lacunar infarct. The mechanism of lacunar infarcts has been a matter of controversies, and at least in some patients, embolism causes lacunes [37].

Our study had some limitations. Firstly, the sample size was small. Some patients could not be studied because of an inadequate insonation window for TCD. It is known that the detection rate of the intracranial artery flow signal using TCD is lower in the Japanese population than in the Caucasian population [38]. The reason why the ratio of men was as high as >90% in this study is thought to be the lack of a temporal window in most old Japanese women, which may be attributed to osteoporosis and the characteristics of the race. Secondly, about 40% of all patients were treated with an anticoagulant and an antiplatelet agent at the time of the TCD study. Although there was no significant difference in anticoagulant and antiplatelet agent use between the MES-positive group and the MES-negative group, such treatment might have influenced the frequency of MES detection.

In conclusion, MES were detected more frequently in the acute phase of stroke in patients with a small cortical and subcortical infarction. The presence of MES may help determine the mechanism of stroke.

Acknowledgment and Funding

References

1 Stork JL, Kimura K, Levi CR, Chambers BR, Abbott AL, Donnan GA: Source of microembolic signals in patients with high-grade carotid stenosis. Stroke 2002;33:2014–2018.

2 Sitzer M, Müller W, Siebler M, Hort W, Kniemeyer HW, Jäncke L, Steinmetz H: Plaque ulceration and lumen thrombus are the main sources of cerebral microemboli in high-grade internal carotid artery stenosis. Stroke 1995;26:1231–1233.

3 Siebler M, Sitzer M, Rose G, Steinmetz H: Microembolism in carotid artery disease. Echocardiography 1996;13:529–536.

4 Siebler M, Kleinschmidt A, Sitzer M, Steinmetz H, Freund HJ: Cerebral microembolism in symptomatic and asymptomatic high-grade internal carotid artery stenosis. Neurology 1994;44:615–618.

5 Siebler M, Sitzer M, Steinmetz H: Detection of intracranial emboli in patients with symptomatic extracranial carotid artery disease. Stroke 1992;23:1652–1654.

6 Levi CR, O'Malley HM, Fell G, Roberts AK, Hoare MC, Royle JP, Chan A, Beiles BC, Chambers BR, Bladin CF, Donnan GA: Transcranial Doppler detected cerebral microembolism following carotid endarterectomy: high microembolic signal loads predict postoperative cerebral ischaemia. Brain 1997;120:621–629.

7 Kumral E, Balkir K, Uzuner N, Evyapan D, Nalbantgil S: Microembolic signal detection in patients with symptomatic and asymptomatic lone atrial fibrillation. Cerebrovasc Dis 2001;12:192–196.

8 Grosset DG, Georgiadis D, Abdullah I, Bone I, Lees KR: Doppler emboli signals vary according to stroke subtype. Stroke 1994;25:382–384.

9 Georgiadis D, Grosset DG, Kelman A, Faichney A, Lees KR: Prevalence and characteristics of intracranial microemboli signals in patients with different types of prosthetic cardiac valves. Stroke 1994;25:587–592.

10 Babikian VL, Hyde C, Pochay V, Winter MR: Clinical correlates of high-intensity transient signals detected on transcranial Doppler sonography in patients with cerebrovascular disease. Stroke 1994;25:1570–1573.

11 Delcker A, Schnell A, Wilhelm H: Microembolic signals and clinical outcome in patients with acute stroke – a prospective study. Eur Arch Psychiatry Clin Neurosci 2000;250:1–5.

12 Serena J, Segura T, Castellanos M, Dávalos A: Microembolic signal monitoring in hemispheric acute ischaemic stroke: a prospective study. Cerebrovasc Dis 2000;10:278–282.

13 Batista P, Oliveira V, Ferro JM: The detection of microembolic signals in patients at risk of recurrent cardioembolic stroke: possible therapeutic relevance. Cerebrovasc Dis 1999; 9:314–319.

14 Droste DW, Ritter M, Kemény V, Schulte-Altedorneburg G, Ringelstein EB: Microembolus detections at follow-up in 19 patients with acute stroke: correlation with stroke etiology and antithrombotic treatment. Cerebrovasc Dis 2000;10:272–277.

15 Daffertshofer M, Ries S, Schminke U, Hennerici M: High-intensity transient signals in patients with cerebral ischemia. Stroke 1996; 27:1844–1849.

16 Sliwka U, Lingnau A, Stohlmann WD, Schmidt P, Mull M, Diehl RR, Noth J: Prevalence and time course of microembolic signals in patients with acute stroke: a prospective study. Stroke 1997;28:358–363.

17 Gao S, Wong KS, Hansberg T, Lam WW, Droste DW, Ringelstein EB: Microembolic signal predicts recurrent cerebral ischemic events in acute stroke patients with middle cerebral artery stenosis. Stroke 2004;35: 2832–2836.

18 Spencer MP, Thomas GI, Nicholls SC, Sauvage LR: Detection of middle cerebral artery emboli during carotid endarterectomy using transcranial Doppler ultrasonography. Stroke 1990;21:415–423.

19 Müller M, Ciccotti P, Axmann C, Kreissler-Haag D: Embolic cerebral ischemia in carotid surgery: a model for human embolic stroke? Med Sci Monit 2003;9:CR411–CR416.

20 Warach S, Gaa J, Siewert B, Wielopolski P, Edelman RR: Acute human stroke studied by whole brain echo planar diffusion-weighted magnetic resonance imaging. Ann Neurol 1995;37:231–241.

21 Gass A, Ay H, Szabo K, Koroshetz WJ: Diffusion-weighted MRI for the 'small stuff': the details of acute cerebral ischaemia. Lancet Neurol 2004;3:39–45.

22 Lovblad KO, Laubach HJ, Baird AE, Curtin F, Schlaug G, Edelman RR, Warach S: Clinical experience with diffusion-weighted MR in patients with acute stroke. AJNR Am J Neuroradiol 1998;19:1061–1066.

23 Gonzalez RG, Schaefer PW, Buonanno FS, Schwamm LH, Budzik RF, Rordorf G, Wang B, Sorensen AG, Koroshetz WJ: Diffusion-weighted MR imaging: diagnostic accuracy in patients imaged within 6 h of stroke symptom onset. Radiology 1999;210:155–162.

24 Kimura K, Minematsu K, Koga M, Arakawa R, Yasaka M, Yamagami H, Nagatsuka K, Naritomi H, Yamaguchi T: Microembolic signals and diffusion-weighted MR imaging abnormalities in acute ischemic stroke. AJNR Am J Neuroradiol 2001;22:1037–1042.

25 Wong KS, Gao S, Chan YL, Hansberg T, Lam WW, Droste DW, Kay R, Ringelstein EB: Mechanisms of acute cerebral infarctions in patients with middle cerebral artery stenosis: a diffusion-weighted imaging and microemboli monitoring study. Ann Neurol 2002;52:74–81.

26 Lyden P, Brott T, Tilley B, Mascha EJ, Levine S, Haley EC, Grotta J, Marler J: Improved reliability of the NIH Stroke Scale using video training. NINDS TPA Stroke Study Group. Stroke 1994;25:2220–2226.

27 Consensus Committee of the 9th International Cerebral Hemodynamic Symposium: Basic identification criteria of Doppler microembolic signals. Stroke 1995;26:1123.

28 North American Symptomatic Carotid Endarterectomy Trial Collaborators: Beneficial effect of carotid endarterectomy in symptomatic patients with high-grade carotid stenosis. N Engl J Med 1991;325:445–453.

29 Bogousslavsky J, Regli F: Centrum ovale infarcts: subcortical infarction in the superficial territory of the middle cerebral artery. Neurology 1992;42:1992–1998.

30 Del Sette M, Eliasziw M, Streifler JY, Hachinski VC, Fox AJ, Barnett HJ: Internal border-zone infarction: a marker for severe stenosis in patients with symptomatic internal carotid artery disease. For the North American Symptomatic Carotid Endarterectomy (NASCET) Group. Stroke 2000;31:631–636.

31 Lee PH, Bang OY, Oh SH, Joo IS, Huh K: Subcortical white matter infarcts: comparison of superficial perforating artery and internal border-zone infarcts using diffusion-weighted magnetic resonance imaging. Stroke 2003;34:2630–2635.

32 Baird AE, Lovblad KO, Schlaug G, Edelman RR, Warach S: Multiple acute stroke syndrome: marker of embolic disease? Neurology 2000;54:674–678.

33 Kang DW, Chalela JA, Ezzeddine MA, Warach S: Association of ischemic lesion patterns on early diffusion-weighted imaging with TOAST stroke subtypes. Arch Neurol 2003;60:1730–1734.

34 Yonemura K, Kimura K, Minematsu K, Uchino M, Yamaguchi T: Small centrum ovale infarcts on diffusion-weighted magnetic resonance imaging. Stroke 2002;33:1541–1544.

35 Wong KS, Gao S, Lam WW, Chan YL, Kay R: A pilot study of microembolic signals in patients with middle cerebral artery stenosis. J Neuroimaging 2001;11:137–140.

36 Momjian-Mayor I, Baron JC: The pathophysiology of watershed infarction in internal carotid artery disease: review of cerebral perfusion studies. Stroke 2005;36:567–577.

37 Futrell N: Lacunar infarction: embolism is the key. Stroke 2004;35:1778–1779.

38 Itoh T, Matsumoto M, Handa N, Maeda H, Hougaku H, Hashimoto H, Etani H, Tsukamoto Y, Kamada T: Rate of successful recording of blood flow signals in the middle cerebral artery using transcranial Doppler sonography. Stroke 1993;24:1192–1195.

Nakajima/Kimura/Shimode/Miyashita/
Uchino/Naritomi/Minematsu

Granulocyte colony-stimulating factor has a negative effect on stroke outcome in a murine model

Akihiko Taguchi,[1] Zhongmin Wen,[1] Kazunori Myojin,[1] Tomoyuki Yoshihara,[1] Takayuki Nakagomi,[2] Daisuke Nakayama,[1] Hidekazu Tanaka,[3] Toshihiro Soma,[4] David M. Stern,[5] Hiroaki Naritomi[1] and Tomohiro Matsuyama[2]

[1]Department of Cerebrovascular Disease, National Cardiovascular Center, 5-7-1 Fujishiro-dai, Suita, Osaka, Japan, 565-8565
[2]Department of Advanced Medicine, Hyogo College of Medicine, Hyogo, Japan
[3]Department of Pharmacology, Graduate School of Medicine, Osaka University, Osaka, Japan
[4]Department of Hematology, Osaka Minami National Hospital, Osaka, Japan
[5]Dean's Office, College of Medicine, University of Cincinnati, OH, USA

Abstract

The administration of CD34-positive cells after stroke has been shown to have a beneficial effect on functional recovery by accelerating angiogenesis and neurogenesis in rodent models. Granulocyte colony-stimulating factor (G-CSF) is known to mobilize CD34-positive cells from bone marrow and has displayed neuroprotective properties after transient ischemic stress. This led us to investigate the effects of G-CSF administration after stroke in mouse. We utilized permanent ligation of the M1 distal portion of the left middle cerebral artery to develop a reproducible focal cerebral ischemia model in CB-17 mice. Animals treated with G-CSF displayed cortical atrophy and impaired behavioral function compared with controls. The negative effect of G-CSF on outcome was associated with G-CSF induction of an exaggerated inflammatory response, based on infiltration of the peri-infarction area with CD11b-positive and F4/80-positive cells. Although clinical trials with G-CSF have been started for the treatment of myocardial and limb ischemia, our results indicate that caution should be exercised in applying these results to cerebral ischemia.

Introduction

Granulocyte colony-stimulating factor (G-CSF) was identified in 1975 and has been broadly used for mobilizing granulocytes from bone marrow (Weaver *et al.*, 1993). G-CSF is also known to mobilize immature hematopoietic cells that include endothelial progenitor cells (EPCs) (Willing *et al.*, 2003). In view of the capacity of circulating EPCs to enhance neovascularization of ischemic tissues (Asahara *et al.*, 1997), the results of recent studies demonstrating that infusion of EPCs accelerates angiogenesis at ischemic sites, thereby limiting tissue injury, is not unexpected (Dzau *et al.*, 2005). As a potential extension of this concept, administration of G-CSF has been shown to accelerate angiogenesis in animal models of limb and myocardial ischemia (Minatoguchi *et al.*, 2004). These observations have provided a foundation for clinical trials testing the effects of G-CSF in limb and myocardial ischemia (Kuethe *et al.*, 2004).

Stroke, a critical ischemic disorder in which there are important opportunities for neuroprotective therapies, is another situation in which enhanced angiogenesis might be expected to improve outcome. For example, we have shown that the administration of CD34-positive cells after stroke accelerates angiogenesis and, subsequently, neurogenesis (Taguchi *et al.*, 2004). Similarly, erythropoietin (EPO), also known to have angiogenic properties, has been shown to have beneficial effects in experimental cerebral ischemia (Ehrenreich *et al.*, 2002; Wang *et al.*, 2004). In addition, G-CSF displays neuroprotective

properties *in vitro* (Schabitz *et al.*, 2003) and *in vivo* (Schabitz *et al.*, 2003; Shyu *et al.*, 2004; Gibson *et al.*, 2005), the latter in a rodent model of transient cerebral ischemic damage. Models of transient cerebral ischemia allow subtle assessment of neuroprotective properties, such as the survival of vulnerable neuronal populations in the penumbra. However, functional outcome after stroke is also determined by inflammation and reparative processes consequent to extensive brain necrosis, the latter better modelled by permanent cerebral ischemia. We have evaluated the effect of G-CSF on stroke outcome in a model of permanent cerebral ischemia with massive cell necrosis. Our model employs permanent ligation of the left middle cerebral artery (MCA) and results in extensive neuronal death in the ischemic zone, as well as more selective apoptotic cell death in the penumbral area (Walther *et al.*, 2002). Using this model, we have tested the effect of G-CSF on functional recovery after stroke.

Materials and methods

All procedures were performed under the auspices of an approved protocol of the Japanese National Cardiovascular Center Animal Care and Use Committees (protocol no. 06026, approval date, May 22, 2006).

Induction of focal cerebral ischemia

To assess the effect of G-CSF on stroke, we developed a highly reproducible murine stroke model applying our previous method

(Taguchi *et al.*, 2004) to CB-17 mice (Clea, Tokyo, Japan). Under halothane anesthesia (inhalation of 3%), the left zygoma was dissected to visualize the MCA through the cranial bone. A hole was made using a dental drill in the bone (diameter 1.5 mm) and the MCA was carefully isolated, electro-cauterized and disconnected just distal to its crossing of the olfactory tract (distal M1 portion). Cerebral blood flow in the MCA area was monitored as described previously (Matsushita *et al.*, 1998). Briefly, an acrylate column was attached to the intact skull using stereotactic coordinates (1 mm anterior and 3 mm lateral to the bregma) and cerebral blood flow was assessed using a linear probe (1 mm in diameter) by laser Doppler flowmetry (Neuroscience Co. Ltd, Osaka, Japan). Mice that showed decreased cerebral blood flow by ~75% immediately after the procedure were used for experiments (success rate of > 95%). Body temperature was maintained at 36.5–37 °C using a heat lamp (Nipponkoden, Tokyo, Japan) during the operation and for 2 h after MCA occlusion. At later timepoints, mice were first subjected to behavioral tests and then to histological examination of their brains. For histological examination, mice were perfusion-fixed with 100 mL of periodate-lysine-paraformaldehyde fixative under deep (pentobarbital) anesthesia (100 mg/kg, intraperitonealy) and their brains were removed. Coronal brain sections (20 μm) were cut on a vibratome (Leica, Solms, Germany) and subjected to immunocytochemistry.

Administration of granulocyte colony-stimulating factor and erythropoietin following stroke

To examine the effect of G-CSF on ischemic cerebral injury, human recombinant G-CSF (Kirin, Tokyo, Japan) was administered subcutaneously at four doses (0.5, 5, 50 or 250 μg/kg) at 24, 48 and 72 h after induction of stroke. As controls, the same volume of phosphate-buffered saline (PBS) or recombinant human EPO (1000 μg/kg; Kirin), the latter known to have angiogenic properties and a positive effect on stroke outcome (Jaquet *et al.*, 2002), was administered subcutaneously. Other time courses of G-CSF administration, including 1 h after stroke (at doses of 0.5, 5, 50 or 250 μg/kg) and continuous administration (100 μg/kg/day) by micro-osmotic pump (Durect, Cupertino, CA, USA) started 1 h after stroke over 7 days, were also studied. To exclude possible effects of an immune response to human recombinant G-CSF in the mouse, murine recombinant G-CSF (R & D Systems, Minneapolis, MN, USA; doses of 0.5, 5 or 50 μg/kg) was administered subcutaneously at 24, 48 and 72 h after induction of stroke, as indicated.

Immunohistochemistry

To evaluate the inflammatory response following administration of G-CSF post-stroke, brain sections were studied immunohistochemically using antibody to CD11b (BD Biosciences, San Jose, CA, USA) and F4/80 (Serotec, Raleigh, NC, USA). The numbers of CD11b-positive inflammatory cells at the anterior cerebral artery (ACA)/MCA border of the infarcted area and numbers of F4/80-positive (F4/80$^+$) activated microglia/macrophages in the ACA area at the exact center of the forebrain section (at the midpoint of the left forebrain, as shown with an orange line in Fig. 1J) were scored by two investigators blinded to the experimental protocol.

Analysis of the peri-infarction and infarcted area after middle cerebral artery occlusion

To investigate mechanisms of brain damage/atrophy consequent to administration of G-CSF, neovessel formation and the extent of

infarction were analysed. Formation of new vessels was assessed at the border of the MCA and ACA territories by perfusing carbon black (0.5 mL; Fuekinori, Osaka, Japan) via the left ventricle of the heart. Staining with 2,3,5-triphenyltetrazolium (TTC) (Sigma-Aldrich, St Louis, MO, USA) was employed to demarcate the border of viable/non-viable tissue. Semiquantitative analysis of angiogenesis employed an angiographic score. Briefly, microscopic digital images were scanned into a computer (Keyence, Osaka, Japan) and the number of carbon black-positive microvessels crossing the border zone of the TTC-negative MCA area to the TTC-positive ACA area was determined. To evaluate the infarcted area 3 days after stroke, coronal brain sections at the exact center of the forebrain were stained with TTC. The infarcted area was measured using a microscopic digital camera system (Olympus, Tokyo, Japan). Infarction in this stroke model was highly reproducible and limited to the left cortex. NIH IMAGE software was used to quantify the TTC-positive area in the ACA territory. A brain atrophy index was established using whole brain images captured by a digital camera system (Olympus). The length of the forebrain was measured along the *x* and *y* dimensions shown in Fig. 1J and the ratio of *x* : *y* was defined as the brain atrophy index.

Behavioral analysis

To assess cortical function, mice were subjected to behavioral testing using the open field task (Kimble, 1968) at 35 days after stroke. In this behavioral paradigm, animals were allowed to search freely in a square acrylic box (30 × 30 cm) for 60 min. A light source on the ceiling of the enclosure was on during the first 30 min (light period) and was turned off during a subsequent 30-min period. On the X- and Y-banks of the open field, two infrared beams were mounted 2 cm above the floor, spaced at 10 cm intervals, forming a flip–flop circuit between them. The total number of beam crossings by the animal was counted and scored as traveling behavior (locomotion). Twelve infrared beams were set 5 cm above the floor, spaced at 3 cm intervals, on the X-bank and the total number of beam crossings was counted and scored as rearing behavior (rearing). To exclude the contribution of physical deficits directly related to the operative procedure and induction of stroke, motor deficiencies were examined on day 35 after stroke. Neurological deficits were scored on a three-point modified scale as described previously (Tamatani *et al.*, 2001): 0, no neurological deficit; 1, failure to extend the left forepaw fully; 2, circling to left and 3, loss of walking or righting reflex. Body weight, monitored in each experimental group, displayed no significant differences (data not shown).

Data analysis

Statistical comparisons among groups were determined using one-way ANOVA and the Dunnett test was used for post-hoc analysis to compare with PBS controls. Where indicated, individual comparisons were performed using Student's *t*-test. In all experiments, mean ± SEM is reported.

Results

Induction of stroke in CB-17 mice

In a previous report, we demonstrated reproducible strokes in severe combined immunodeficient (SCID) mice by permanent ligation of the left MCA (Taguchi *et al.*, 2004). As SCID mice originated from the CB-17 strain, we expected anatomical similarity of cerebral arteries in
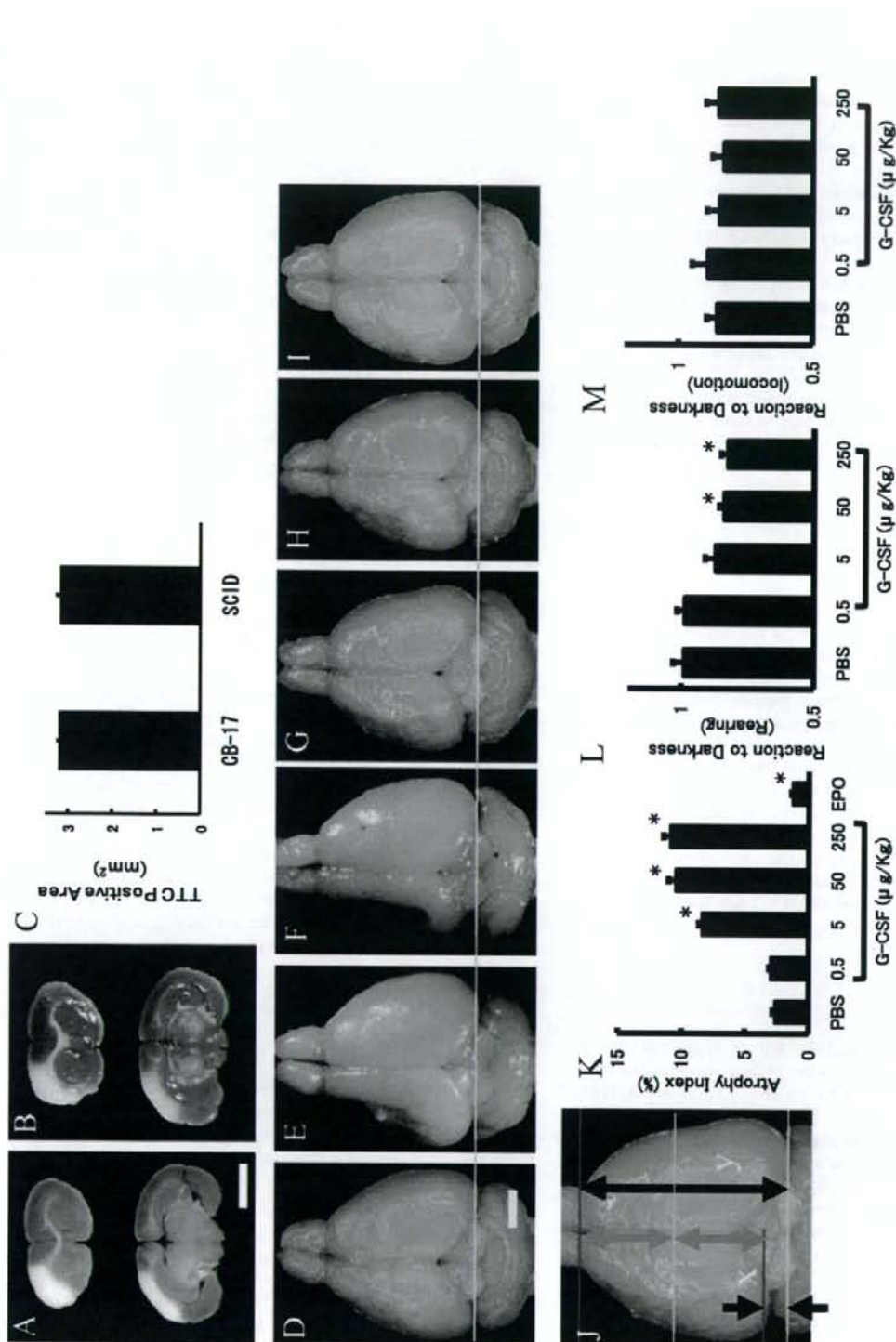
Fig. 1. Administration of granulocyte colony-stimulating factor (G-CSF) induces cortical atrophy. (A–C) Induction of stroke by ligation of the M1 portion of the left middle cerebral artery (MCA). Forebrain sections harvested from mice 3 h after stroke were stained with 2,3,5-triphenyltetrazolium (TTC), and lack of positive staining is observed in the MCA cortex of CB-17 (A) and severe combined immunodeficient (SCID) mice (B). The TTC-positive anterior cerebral artery area at the exact center of forebrain was quantified using NIH IMAGE (C). A highly reproducible TTC-positive (surviving) cortical area was observed in CB-17 and SCID mice. (D–I) On day 35 post-stroke, brains were evaluated grossly. Compared with post-stroke mice treated with phosphate-buffered saline (PBS) (D), no significant difference was observed in mice treated with 0.5 μg/kg of G-CSF (E). In contrast, brain atrophy was observed with G-CSF treatment at doses of 5 μg/kg (F), 50 μg/kg (G) or 250 μg/kg (H). Treatment with erythropoietin (EPO) (I) had a beneficial effect in terms of brain atrophy. Note that, compared with the contralateral side (green line), atrophy in the longitudinal direction was observed in animals treated with G-CSF (F–H). (J) A brain atrophy index was defined as the ratio of x : y. (K) ANOVA analysis (n = 6 per group) revealed significant brain atrophy in mice at doses of G-CSF above 0.5 μg/kg. In contrast, a reduction of brain atrophy was observed in mice treated with EPO. (L and M) Behavioral analysis post-stroke. ANOVA analysis (n = 6 per group) in mice subjected to stroke revealed that treatment with either 50 or 250 μg/kg of G-CSF significantly impaired the rearing response compared with PBS (L), although no significant difference was observed in locomotion (M). Marker bars, 2 mm (A and D). *P < 0.05 vs. PBS.

these two strains. Strokes were induced in CB-17 mice by permanent ligation of the M1 distal portion of the left MCA. To evaluate the infarcted area, brain sections were stained with TTC at 3 h after stroke. Reproducible strokes were induced in CB-17 mice (Fig. 1A) that were similar to those in SCID mice (Fig. 1B). The surviving cortical area post-stroke, represented by the TTC-positive ACA area at the exact center of forebrain, was also similar in CB-17 and SCID mice (Fig. 1C, $n = 6$/species).

Granulocyte colony-stimulating factor accelerates brain injury after stroke

In a previous study, we demonstrated that enhanced neovascularization post-stroke, due to administration of CD34-positive cells, promoted neuronal regeneration leading to cortical expansion and functional recovery (Taguchi et al., 2004). As G-CSF is known to mobilize CD34-positive cells from bone marrow (Kuethe et al., 2004), we investigated the effects of G-CSF treatment, starting 24 h after stroke and continuing for 3 days, using the above permanent focal cerebral ischemia model. Compared with control animals receiving PBS alone (Fig. 1D), no significant difference was observed in mice that received 0.5 μg/kg of G-CSF (Fig. 1E and K) at 35 days after stroke. However, remarkable brain atrophy was observed with G-CSF treatment at 5 μg/kg (Fig. 1F and K), 50 μg/kg (Fig. 1G and K) or 250 μg/kg (Fig. 1H and K). In contrast, a mild protective effect, with respect to brain atrophy, was observed in the group treated with EPO post-stroke (1000 μg/kg; Fig. 1I and K). In each condition depicted in Fig. 1, a representative image is shown and quantitative analysis of the brain atrophy index ($n = 6$/experimental condition; defined in Fig. 1J) is demonstrated in Fig. 1K.

Granulocyte colony-stimulating factor has a negative effect on functional recovery after stroke

To investigate functional recovery in animals treated with G-CSF, we performed behavioral testing on day 35 after stroke ($n = 6$, for each group). Compared with post-stroke CB-17 mice that received PBS, mice treated with 50 or 250 μg/kg G-CSF displayed impaired behavioral function as assessed by the 'dark' response, with respect to rearing (Fig. 1L and Table 1) analysed by ANOVA followed by post-hoc Dunnett test, although there was no significant change in locomotion (Fig. 1M). In contrast, treatment with EPO accelerated functional recovery with respect to both rearing (1.18 ± 0.07 and 0.99 ± 0.04 in EPO and PBS groups, respectively, $n = 6$ per group, $P < 0.05$) and locomotion (1.04 ± 0.04 and 0.85 ± 0.04 in EPO and PBS groups, respectively, $n = 6$ per group, $P < 0.05$). Mice showed rapid recovery from focal motor deficits and, by day 16 post-stroke, no motor deficits were detected based on a modified three-point scale (not shown).

Granulocyte colony-stimulating factor accelerates angiogenesis after stroke

Increased brain atrophy and impaired functional recovery in animals treated with G-CSF post-stroke were quite unexpected because of the known ability of G-CSF to mobilize CD34-positive cells from bone marrow (Willing et al., 2003). In addition, a previous study showed neuroprotective properties of G-CSF in models of transient cerebral ischemia (Schabitz et al., 2003). These considerations led us to analyse mechanisms contributing to increased brain atrophy after

TABLE 1. Raw data of open field test (G-CSF rearing)

Treatment and individual	Rearing (counts)		Reaction to darkness (Right OFF/Right ON)
	Right ON	Right OFF	
PBS			
1	662	640	0.97
2	611	708	1.16
3	487	450	0.92
4	587	540	0.92
5	482	430	0.89
6	425	450	1.06
Mean ± SEM	542.3 ± 37.2	536.3 ± 47.1	0.99 ± 0.04
G-CSF (0.5μg/kg)			
1	600	562	0.94
2	601	650	1.08
3	494	425	0.86
4	731	731	1.00
5	767	784	1.02
6	498	501	1.01
Mean ± SEM	615.2 ± 46.7	608.8 ± 56.2	0.98 ± 0.03
G-CSF (5μg/kg)			
1	577	497	0.86
2	537	368	0.69
3	310	288	0.93
4	520	485	0.93
5	673	652	0.97
6	572	480	0.84
Mean ± SEM	531.5 ± 49.3	461.7 ± 50.8	0.87 ± 0.04
G-CSF (50μg/kg)			
1	592	520	0.88
2	463	376	0.81
3	478	430	0.90
4	307	250	0.81
5	484	410	0.85
6	385	295	0.77
Mean ± SEM	451.5 ± 39.6	380.2 ± 39.6	0.84 ± 0.02
G-CSF (250μg/kg)			
	578	424	0.73
	501	401	0.80
	507	380	0.75
	465	412	0.89
	380	341	0.90
	401	347	0.87
Mean ± SEM	472 ± 29.9	384.2 ± 14.0	0.82 ± 0.03

Right ON, under light condition; Right OFF, under dark condition.

administration of G-CSF. As G-CSF has been reported to accelerate angiogenesis in limb and cardiac models of ischemic injury (Minatoguchi et al., 2004), we sought to determine its impact on neovascularization in our permanent focal cerebral infarction model. Compared with PBS-treated controls (Fig. 2A), increased neovasculature at the border of the MCA and ACA cortex (staining with TTC demarcates viable/non-viable tissue and carbon black was used to visualize vessels) was observed in animals treated with G-CSF (50 μg/kg, Fig. 2B). Assessment of the angiographic score confirmed the impression of increased neovasculature in animals treated with G-CSF, compared with the group receiving PBS (Fig. 2C; $P < 0.05$).

Next, we investigated possible neuroprotective properties of G-CSF after stroke. Analysis of the infarcted/surviving area 3 days after stroke was evaluated in animals treated with PBS (Fig. 2D) or G-CSF (50 μg/kg, Fig. 2E) based on TTC staining; there was no effect of G-CSF treatment compared with controls receiving PBS (Fig. 2F). Thus, G-CSF did not impact on the viability of 'at-risk' tissue in the
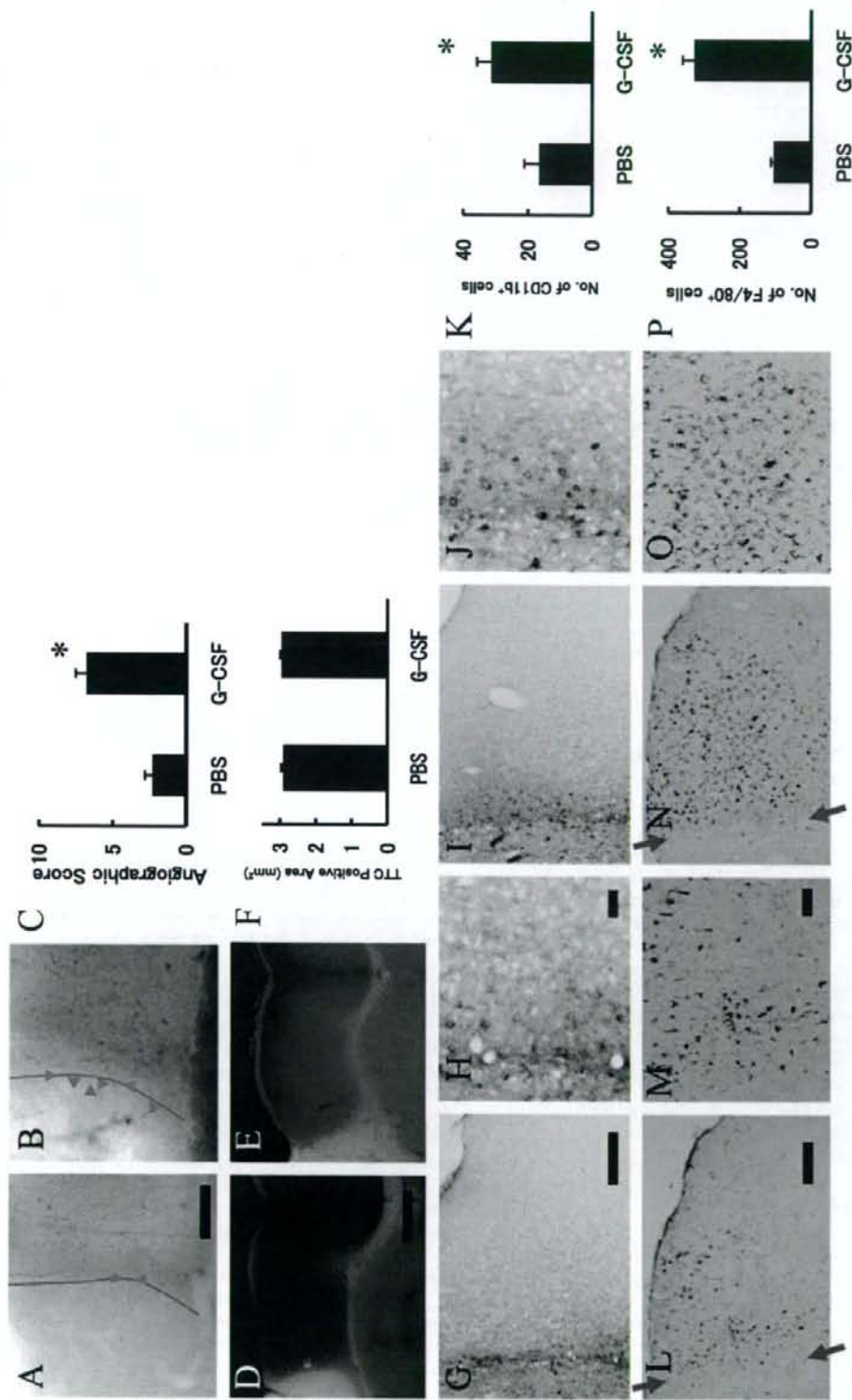
FIG. 2. Administration of granulocyte colony-stimulating factor (G-CSF) after stroke enhances the inflammatory response. (A–C) On day 3 after stroke, mice were infused with carbon black ink. Compared with mice treated with phosphate-buffered saline (PBS) (A), increased neovascularization was observed at the border between anterior cerebral artery (ACA) and middle cerebral artery (MCA) regions in mice treated with G-CSF (B). Representative micrographs are shown. The angiographic score (see Materials and methods) showed increased neovascularization (n = 6 per group) in mice treated with G-CSF post-stroke compared with controls (PBS). (D–F) There was no difference in the 2,3,5-triphenyltetrazolium (TTC)-positive ACA area at the exact center of forebrain comparing post-stroke animals treated with G-CSF (E) and controls/PBS (D). Sections from each animal were subjected to statistical analysis using Student's t-test (n = 6 animals per group; F). (G–K) CD11b-positive cells were visualized in the ACA area in tissue from post-stroke animals treated with PBS (G, lower magnification; H, higher magnification) or G-CSF (I, lower magnification; J, higher magnification). Sections from each animal were evaluated (n = 6 animals per group) and the average number of CD11b-positive cells per high power field is shown in each of the two groups (K). (L–P) F4/80-positive (F4/80⁺) activated macrophages/microglia in mice treated with PBS were relatively limited to the area close to the border of infarcted tissue (L, lower magnification; M, higher magnification). However, an expanded area and increased density of F4/80⁺ cells was observed after administration of G-CSF (N, lower magnification; O, higher magnification). The total number of F4/80⁺ activated macrophages/microglia in the viable ACA area identified on the section at exact center of forebrain was quantified (n = 6 per group) (N). Scale bars: 0.2 mm (A), 1 mm (D), 0.3 mm (G and L) and 30 μm (H and M). *P < 0.05 vs. PBS. Arrowheads (A and B) indicate microvessels at the border of the MCA and ACA cortex (red line). Arrows (L and N) indicate the border of infarcted tissue (left side, stroke MCA area; right side, viable ACA area).

immediate post-stroke period (up to 3 days), although there was a long-term effect on brain atrophy (evaluated at 35 days).

Granulocyte colony-stimulating factor enhances the inflammatory response after stroke

Further studies were performed to analyse the apparent dichotomy between G-CSF-mediated enhancement of neovascularization of the ischemic territory post-stroke vs. increased cerebral atrophy and lack of improvement in behavioral testing. We focused our studies on the inflammatory response. Compared with PBS-treated mice (Fig. 2G, lower magnification; Fig. 2H, higher magnification), increased accumulation of CD11b-positive inflammatory cells, including monocytes and granulocytes (Campanella *et al.*, 2002), was observed in G-CSF-treated mice (50 µg/kg) at the border of the infarcted area (Fig. 2I, lower magnification; Fig. 2J, higher magnification). Quantitative analysis ($n = 6$ each) revealed a significant difference in the number of infiltrating CD-11b-positive cells (Fig. 2K; $P < 0.05$). These results led us to evaluate the presence of activated macrophages/microglia in ischemic lesions, as the latter are known to enhance brain damage after stroke (Mabuchi *et al.*, 2000). Although F4/80+ activated macrophages/microglia were observed in the viable (i.e. non-ischemic) ACA area following treatment with PBS (Fig. 2L, lower magnification; Fig. 2M, higher magnification), increased numbers of F4/80+ macrophages/microglia were observed in post-stroke animals treated with G-CSF (Fig. 2N, lower magnification; Fig. 2O, higher magnification). F4/80+ activated macrophages/microglia in post-stroke mice treated with PBS were principally limited to the area close to the border of the infarcted tissue. In contrast, F4/80+ cells in post-stroke mice treated with G-CSF were observed in a broad area and at higher density in the ACA territory. The total number of F4/80+ cells in a section at the exact center of the forebrain was quantified ($n = 6$ each); a significant increase in F4/80+ activated macrophages/microglia was observed in G-CSF-treated mice, compared with controls receiving PBS post-stroke (Fig. 2P; $P < 0.05$).

Administration of granulocyte colony-stimulating factor 1 h after stroke also induces brain atrophy

As the experimental protocol for the above studies involved G-CSF treatment starting 24 h after stroke, it was important to vary our protocol. For this purpose, we also administered G-CSF within 1 h of stroke (Fig. 3A, $n = 6$ each) or performed continuous treatment for up to 7 days (Fig. 3B, $n = 6$ each). Our results demonstrate induction of brain atrophy in post-stroke animals treated with G-CSF subjected to either of these protocols compared with PBS-treated controls.

To exclude the immune response stimulated by human recombinant G-CSF in mice, various doses of mouse recombinant G-CSF were administered and the effect was determined ($n = 6$ each dose). We found significant brain atrophy with administration of lower doses (0.5 and 5 µg/kg) of recombinant murine G-CSF. As the survival rate was only 50% (three mice dead out of six) with administration of a higher dose (50 µg/kg), the group was excluded from this analysis.
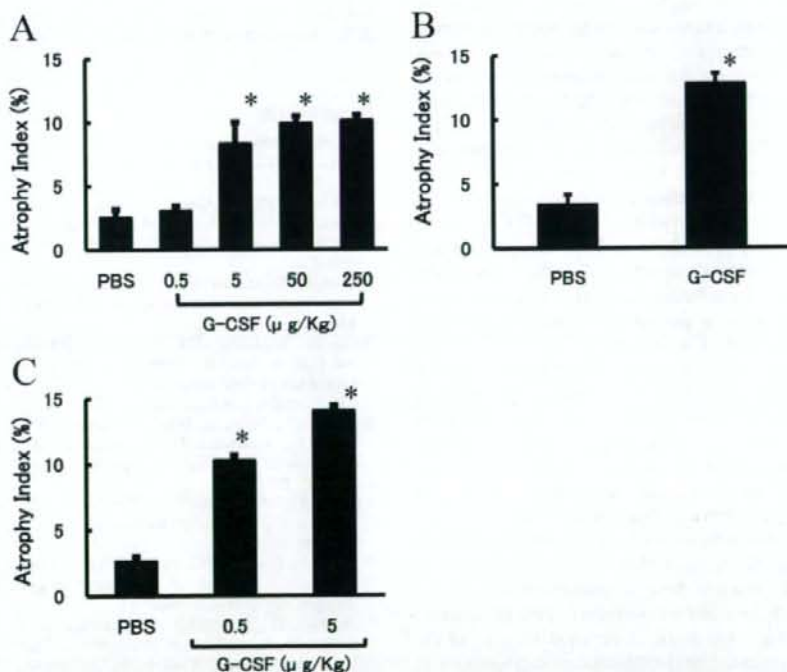

FIG. 3. Effect of granulocyte colony-stimulating factor (G-CSF) on brain atrophy. (A) G-CSF or phosphate-buffered saline (PBS) was administered 1 h after stroke and brains were evaluated grossly on day 35 post-stroke. (B) Continuous administration of G-CSF or PBS starting at 1 h post-stroke for 7 days was also tested. (C) Mouse recombinant G-CSF was administrated at the indicated dose and was found to increase the atrophy index. In each case, $n = 6$ per group. *$P < 0.05$ vs. PBS.

Discussion

Our results demonstrate that, in a murine permanent focal cerebral infarction model, administration of G-CSF, either human or murine recombinant, post-stroke is associated with enhanced brain atrophy.

In order to evaluate experimental treatments for stroke, reproducible induction of cerebral ischemia/infarction is a prerequisite. Previously, we developed a stroke model using SCID mice (Taguchi *et al.*, 2004) that proved suitable for quantification of the effect of cell therapy on neurogenesis, neovessel formation and neural function. In the current study, we have applied this stroke model to CB-17 mice and found it to provide highly reproducible data.

Granulocyte colony-stimulating factor is known to mobilize EPCs from bone marrow (Willing *et al.*, 2003) and accelerate angiogenesis (Bussolino *et al.*, 1991). Clinical studies have demonstrated that administration of G-CSF has beneficial effects in patients with acute myocardial infarction, including promotion of neovascularization and improvement of perfusion (Kuethe *et al.*, 2004). In addition, G-CSF has been shown to display neuroprotective properties in a rodent model (Schabitz *et al.*, 2003). Based on these observations, G-CSF has been tested in animal models of transient cerebral ischemia and beneficial effects have been reported (i.e. reduced infarct volume and enhanced functional recovery) (Schabitz *et al.*, 2003; Shyu *et al.*, 2004; Gibson *et al.*, 2005). In the current study, we employed a permanent cerebral infarction (i.e. stroke) model, rather than a model of transient ischemia, to investigate the effects of G-CSF.

In addition to its effects on EPCs, G-CSF is known to mobilize granuloctyes from the bone marrow, and these granulocytes have been shown to become associated with endothelia and accumulate in the ischemic brain (Justicia *et al.*, 2003). These observations suggested the possibility that G-CSF might augment the inflammatory response consequent to ischemic tissue damage by promoting recruitment and activation of neutrophils and mononuclear-derived cells (blood monocytes, monocyte-derived macrophages and microglia) (Zawadzka & Kaminska, 2005). Consistent with this concept, accumulation of CD11b-positive inflammatory cells at the border of the infarcted area was observed after treatment with G-CSF. Furthermore, a striking increase in the number of F4/80⁺ activated macrophages/microglia was observed in non-ischemic surviving tissue (adjacent to the infarct) subsequent to administration of G-CSF. The inflammatory response after stroke has been shown to have both positive and negative effects on tissue repair (Fontaine *et al.*, 2002). Our results indicated that the balance of these inflammatory mechanisms on stroke outcome in the mouse using a permanent ischemia model and following administration of G-CSF is negative.

It would appear that the current work contradicts previous studies showing a positive effect of G-CSF after myocardial ischemia (Minatoguchi *et al.*, 2004). This apparent discrepancy may be explained, at least in part, by differences in brain and cardiac vasculature. Non-ischemic brain is protected from the systemic inflammatory response by an intact blood–brain barrier composed of endothelia joined by tight junctions. Thus, invasion of the central nervous system by activated inflammatory cells is largely prevented and the neural system functions within a relatively protected microenvironment, with respect to the inflammatory response (Neumann, 2000). However, stroke disturbs the integrity of the blood–brain barrier. We propose that a combination of impaired function of the blood–brain barrier in the context of G-CSF-induced augmentation of the inflammatory response in ischemic tissue contributes to the observed brain atrophy. Although activated inflammatory cells are known to participate in both the injurious and healing processes (Minatoguchi *et al.*, 2004), our results indicate an overall negative

effect on neural function and neurogenesis following treatment with G-CSF in the post-stroke period.

In contrast to G-CSF, EPO had beneficial effects after stroke in the current model. Such positive effects are consistent with previous reports (Bernaudin *et al.*, 1999; Bahlmann *et al.*, 2004; Bartesaghi *et al.*, 2005; Kretz *et al.*, 2005) demonstrating that EPO promotes mobilization of EPCs (Bahlmann *et al.*, 2004), has angiogenic (Jaquet *et al.*, 2002) and neuroprotective properties (Bartesaghi *et al.*, 2005), and accelerates regeneration (Kretz *et al.*, 2005).

Taken together, our results indicate that administration of G-CSF after stroke results in an exaggerated inflammatory response, both at the border of the ischemic region and also in non-ischemic brain tissue, and that this is associated with brain atrophy and poor neural function. Thus, we suggest that a cautious approach should be taken in applying results of studies with G-CSF in the peripheral circulation (i.e. limb and cardiac ischemia) to the setting of cerebral ischemia. In a more general context, it is possible that agents with pro-inflammatory properties will prove less useful as therapeutic agents in cerebral ischemia in view of the above observations.

Acknowledgements

Abbreviations

ACA, anterior cerebral artery; EPC, endothelial progenitor cell; EPO, erythropoietin; F4/80⁺, F4/80-positive; G-CSF, granulocyte colony-stimulating factor; MCA, middle cerebral artery; PBS, phosphate-buffered saline; SCID, severe combined immunodeficient; TTC, 2,3,5-triphenyltetrazolium.

References

Asahara, T., Murohara, T., Sullivan, A., Silver, M., van der Zee, R., Li, T., Witzenbichler, B., Schatteman, G. & Isner, J.M. (1997) Isolation of putative progenitor endothelial cells for angiogenesis. *Science*, **275**, 964–967.

Bahlmann, F.H., De Groot, K., Spandau, J.M., Landry, A.L., Hertel, B., Duckert, T., Boehm, S.M., Menne, J., Haller, H. & Fliser, D. (2004) Erythropoietin regulates endothelial progenitor cells. *Blood*, **103**, 921–926.

Bartesaghi, S., Marinovich, M., Corsini, E., Galli, C.L. & Viviani, B. (2005) Erythropoietin: a novel neuroprotective cytokine. *Neurotoxicology*, **26**, 923–928.

Bernaudin, M., Marti, H.H., Roussel, S., Divoux, D., Nouvelot, A., MacKenzie, E.T. & Petit, E. (1999) A potential role for erythropoietin in focal permanent cerebral ischemia in mice. *J. Cereb. Blood Flow Metab.*, **19**, 643–651.

Bussolino, F., Ziche, M., Wang, J.M., Alessi, D., Morbidelli, L., Cremona, O., Bosia, A., Marchisio, P.C. & Mantovani, A. (1991) In vitro and in vivo activation of endothelial cells by colony-stimulating factors. *J. Clin. Invest.*, **87**, 986–995.

Campanella, M., Sciorati, C., Tarozzo, G. & Beltramo, M. (2002) Flow cytometric analysis of inflammatory cells in ischemic rat brain. *Stroke*, **33**, 586–592.

Dzau, V.J., Gnecchi, M., Pachori, A.S., Morello, F. & Melo, L.G. (2005) Therapeutic potential of endothelial progenitor cells in cardiovascular diseases. *Hypertension*, **46**, 7–18.

Ehrenreich, H., Hasselblatt, M., Dembowski, C., Cepek, L., Lewczuk, P., Stiefel, M., Rustenbeck, H.H., Breiter, N., Jacob, S., Knerlich, F., Bohn, M., Poser, W., Ruther, E., Kochen, M., Gefeller, O., Gleiter, C., Wessel, T.C., De Ryck, M., Itri, L., Prange, H., Cerami, A., Brines, M. & Siren, A.L. (2002) Erythropoietin therapy for acute stroke is both safe and beneficial. *Mol. Med.*, **8**, 495–505.

Fontaine, V., Mohand-Said, S., Hanoteau, N., Fuchs, C., Pfizenmaier, K. & Eisel, U. (2002) Neurodegenerative and neuroprotective effects of tumor